I.O. STARODUB, Y. ZOLOTARYUK

Bogolyubov Institute for Theoretical Physics, Nat. Acad. of Sci. of Ukraine
(14b, Metrolohichna Str., Kyiv 03143, Ukraine; e-mail: starodub@bitp.kiev.ua, yzolo@bitp.kiev.ua)

FLUXON SCATTERING ON A STRIPE-LIKE IMPURITY IN A TWO-DIMENSIONAL JOSEPHSON JUNCTION

PACS 05.45.Yv, 74.50.+r

The interaction of a soliton (fluxon) with a stripe-like inhomogeneity in a two-dimensional Josephson junction is studied. The radiation emitted due to the fluxon scattering on the impurity is calculated. The total radiation energy shows a distinct resonant dependence as a function of the fluxon velocity. The current-voltage characteristic of such a junction with a fluxon trapped in it is calculated. The signature of the emitted radiation on the current-voltage dependence is analyzed.

K e y w o r d s: fluxon scattering, stripe-like impurity, two-dimensional Josephson junction.

1. Introduction

Nonlinear wave phenomena are ubiquitous in the Nature. Among them, solitons (stable spatially localized waves that travel with constant shape and velocity) take a special place. The existence of a soliton in magnets, liquid crystals, optical fibers, molecular chains, and large Josephson junctions (LJJs) is demonstrated. Solitons in LJJs have the physical meaning of magnetic flux quanta, are also known as *fluxons*, and are described by the well-known sine-Gordon (SG) equation. The fluxon dynamics in LJJs continues to be a subject of the strong theoretical and experimental interest during the last three decades [1–3]. The convenient way to prepare a junction with the required properties is to install various inhomogeneities into it.

Up to now, the substantial theoretical work has been devoted to the study of the fluxon motion in one-dimensional (1D) LJJs with point-like impurities. In the pioneering paper [4], the main results for the dc-driven and damped soliton interaction with an impurity are presented. The radiation emitted during the fluxon-impurity interaction has been computed for the individual impurity [5], multiple randomly distributed impurities [6], and the periodic impurity array [7]. Experimental results on the fluxon scattering on impurities are reported in Refs. [7, 8]. The scattering of a kink on point impurities in the unbiased and non-damped SG model has been studied in Refs. [9, 10]. The absence of dissipation makes the soliton-impurity interaction more complex and strongly dependent on the initial conditions. But in the case of the fluxon dynamics in a LJJ, the presence of the dissipation is unavoidable. As is shown in Ref. [4], the soliton either passes the impurity or gets trapped by it, depending on the value of bias current. Spatially inhomogeneous Josephson systems with trapped fluxons have been discussed as prospective applications, such as fluxon-based information devices [11].

While it is common to consider 1D LJJs, they are always two-dimensional (2D) in reality in the sense that they have a finite width in the direction perpendicular to the fluxon propagation direction. If the junction is quite narrow, the 1D approximation is justifiable. However, it might not be so. Therefore, the presence of the transverse degree of freedom may play an important role. Up to now, most of the research has been focused on the various isotropic 2D structures like oscillons, skyrmions, and ring kinks [12–15]. It is worth mentioning also the case of window junctions [16, 17] that studies the point or rectangular Josephson junctions embedded in a larger two-dimensional superconducting sample. This situation can be viewed as the opposite to the case of the superconducting or insulating impurity embedded in the large Josephson junction, which will be discussed in this paper.

The solitonic front propagation in 2D nonlinear media has been studied in the number of papers. For the lattice acoustic soliton front interaction with mass impurities [18], it has been shown that the front can bypass the point impurity, while a 1D lattice soliton gets reflected from it. Moreover, the soliton front can overcome even the impurity of the infinite mass. The

fluxon front scattering on a δ-like point impurity has been investigated in [19] for the case of an infinite 2D sample. Waves traveling along the 2D sine-Gordon (SG) solitonic front have been investigated in [20].

The motivation of this work is twofold. First of all, it is of interest to investigate the 2D fluxon dynamics in the presence of spatial inhomogeneities, when the junction width is finite. We expect that the fluxon transmission in this case will be significantly enhanced comparing to the pure 1D case. Next, since the impurities have finite sizes in the real systems [8], we are interested in finding how the fluxon in the 2D LJJ interacts with a stripe-like impurity elongated in the direction perpendicular to the direction of the fluxon propagation. In particular, we are going to study the dependence of the fluxon trapping and transmission processes on the junction parameters and to calculate the energy density of the radiation emitted during the fluxon scattering process.

This paper is organized as follows. In the next section, the model is described. Section 3 is devoted to the studies of the radiation emitted due to the fluxon-impurity interaction. In Section 4, we study the fluxon transmission through an impurity as a function of the dc bias. The next section utilizes the results of the previous two sections and is devoted to the current-voltage characteristics of the junction. In the last section, the discussion and conclusions are presented.

2. The Model

We consider a 2D large Josephson junction subjected to an external time-independent bias. The main dynamical variable is a difference between the phases $\theta_2(x,y;t) - \theta_1(x,y;t) = \phi(x,y;t)$ of the macroscopic wave functions of the superconducting layers of the junction. The time evolution of the phase difference is governed by the perturbed sine-Gordon (SG) equation

$$\partial_t^2\phi - \Delta\phi + [1 + f(x,y)]\sin\phi = -\alpha\phi_t - \gamma, \qquad (1)$$

where $\Delta\phi = (\partial_x^2 + \partial_y^2)\phi$. In this dimensionless equation, the spatial variables x and y are normalized to the Josephson penetration depth λ_J, and the temporal variable t is normalized to the inverse Josephson plasma frequency ω_J^{-1} [1, 2]. The bias current γ is normalized to the critical Josephson current of the junction, and α is the dimensionless dissipation parameter. The function $f(x,y)$ describes the spatial inhomogeneity. We consider a stripe-like microshort (i.e., the region of the locally enhanced density of the critical superconducting current) of width d and strength $\mu > 0$, which is stretched along the y direction:

$$f(x,y) = \mu\delta(x)\left[\theta\left(y + \frac{d}{2}\right) + \theta\left(\frac{d}{2} - y\right) - 1\right]. \qquad (2)$$

Here, $\theta(x)$ is the Heaviside function.

In the unperturbed case, the SG equation possesses the soliton solution of the form

$$\phi_0(x,t) = 4\arctan\left[\exp\left(Q\frac{x - vt}{(1-v^2)^{1/2}}\right)\right], \qquad (3)$$

where v is the soliton velocity, and $Q = \pm 1$ is the topological charge. Without loss of generality, we restrict ourselves to the case $Q = 1$. The boundary conditions will be discussed in the next sections.

3. Generation of Radiation by the Fluxon-Impurity Interaction

Fluxon scattering on an obstacle naturally results in the emission of radiation. Assuming the dissipation and the dc bias to be negligible, we consider the radiation emitted by the fluxon that interacts with the stripe impurity (2). The radiation emission studies for the respective 1D problem are based on the inverse-scattering transform [5, 7, 10]. However, we are going to modify the approach developed in Ref. [19].

The solution of the perturbed SG equation (1) is presented as a superposition of the exact soliton solution $\phi_0(x,t)$ [see Eq. (3)] with $Q = 1$ and the radiation on its background: $\phi(x,y,t) = \phi_0(x,t) + \psi(x,y,t)$, $|\psi| \ll 1$. After substituting this ansatz into the SG equation (1) and transferring to the frame of reference $[\xi = (1-v^2)^{-1/2}(x - vt), y, \tau = (1-v^2)^{-1/2}(t - vx)]$ that moves with the fluxon velocity v, one obtains the linearized equation for the radiated waves:

$$[\partial_\tau^2 + \hat{L}]\psi = -F(\xi,y,\tau)\sin[\phi_0(\xi)], \qquad (4)$$

$$\hat{L} \equiv -(\partial_\xi^2 + \partial_y^2) + \cos[\phi_0(\xi)], \qquad (5)$$

$$F(\xi,y,\tau) = \mu(1-v^2)^{1/2}\delta(\xi + v\tau)\left[\theta\left(y + \frac{d}{2}\right) + \theta\left(\frac{d}{2} - y\right) - 1\right]. \qquad (6)$$

The soliton solution in the moving frame is given by $\phi_0(\xi) = 4\arctan(\exp\xi)$. With the help of the eigenfunctions (for the corresponding 1D problem, see Ref. [21]) of the operator $\hat{L}$ on the infinite plane,

$$\varphi(\xi, y; q_\xi, q_y) = \frac{e^{i(q_\xi\xi + q_y y)}}{(2\pi)^{3/2}} \frac{q_\xi + i\tanh\xi}{(1+q_\xi^2)^{1/2}}, \tag{7}$$

the solution of (4) can be represented in the form

$$\psi(\xi, y, \tau) =$$

$$= \int\limits_{-\infty}^{+\infty}\int\limits_{-\infty}^{+\infty} a(q_\xi, q_y; \tau)\varphi(\xi, y; q_\xi, q_y)\ dq_\xi\ dq_y. \tag{8}$$

Here, q_ξ and q_y are the respective components of the radiation wave vector, and the radiation amplitude $a(q_\xi, q_y; \tau)$ is yet to be found. It is more convenient to use another function (see also Ref. [19]), $b(q_\xi, q_y; \tau) \doteq \doteq (\partial_\tau a - i\bar{\omega}a)\exp(i\bar{\omega}\tau)$, where $\bar{\omega} = (1 + q_\xi^2 + q_y^2)^{1/2}$ is the radiated wave frequency in the moving frame. The calculation of $b(q_\xi, q_y; \tau)$ is given in Appendix. We are interested in the final values of the emitted radiation, $B(q_\xi, q_y) = b(q_\xi, q_y; \tau \to +\infty)$. It is assumed that there was no radiation before the fluxon interacted with the impurity. Therefore, finding the final radiation amplitude reduces to the simple integration: $B(q_x, q_y) = \int_{-\infty}^{+\infty} \partial_\tau b(q_x, q_y; \tau)d\tau$. The expression for the derivative $\partial_\tau b$ is given by Eq. (23) in Appendix. This integral can be easily calculated. The total emitted energy density reads $\mathcal{E}(q_\xi, q_y) \simeq 4\pi^{-1}|B(q_\xi, q_y)|^2$ (see Ref. [19] for details). Thus, the final expression for the energy density is

$$\mathcal{E}(q_\xi, q_y) = \frac{8\mu^2}{q_y^2}\sin^2\left(\frac{q_y d}{2}\right)\mathrm{sech}^2\left[\frac{\pi}{2v}(q_\xi v + \bar{\omega})\right] \times$$

$$\times \frac{(1-v^2)}{v^6}\frac{\left[\bar{\omega}^2 - \left(1+q_\xi^2\right)v^2\right]^2}{1+q_\xi^2}. \tag{9}$$

We have to return back to the laboratory frame of reference. This means that the wave-vector components and the radiation frequency must undergo the following transformation:

$$q_x = \frac{q_\xi + v\bar{\omega}}{\sqrt{1-v^2}}, \quad \omega = \frac{vq_\xi + \bar{\omega}}{\sqrt{1-v^2}}, \quad \omega = (1+q_x^2+q_y^2)^{1/2}. \tag{10}$$

The q_y component remains unchanged. As a result, we obtain the energy density in the laboratory frame of reference:

$$\mathcal{E}(q_x, q_y) = \frac{8\mu^2}{q_y^2}\sin^2\left(\frac{q_y d}{2}\right)\mathrm{sech}^2\left[\frac{\pi\omega}{2v}(1-v^2)^{1/2}\right] \times$$

$$\times \frac{(1-v^2)^2}{v^6}\frac{\left[(\omega - vq_x)^2 + (vq_y)^2\right]^2}{(\omega - vq_x)^2 - (1-v^2)q_y^2}. \tag{11}$$

The energy density function for the stripe impurity is symmetric with respect to the transformations $q_y \to -q_y$ and $q_x \to -q_x, v \to -v$. Therefore, it is sufficient to study it for the velocities in the interval $0 \le v < 1$. Its shape for different values of soliton velocity is given in Fig. 1. It should be noted that this dependence has no singularities for all $-\infty < q_{x,y} < +\infty$, because its divisor is always positive, as can easily be seen from Eq. (9). The main peak of the $\mathcal{E}(q_x, q_y)$ dependence lies on the $q_y = 0$ axis. In the limit $v \to 0$, the dependence becomes almost isotropic and strongly localized around the main peak, which moves toward the origin, as v is decreased. The increase in v leads to the squeezing of the main peak in the q_y direction and its elongation in the q_x direction. The maximum of $\mathcal{E}(q_x, q_y)$ moves toward the negative values of q_x. The secondary peaks that exist due to the presence of the sin term in Eq. (11) become noticeable, when $v \to 1$ (see Fig. 1, *c*). The functional dependence of the energy density function for the stripe impurity differs from the same dependence for the point impurity $f(x, y) = \mu_*\delta(x)\delta(y)$ studied in Ref. [19] (see Eq. (2.16) of that paper) only by the presence of the term $\sin^2(q_y d/2)/q_y^2$. This term, however, changes drastically the properties of the energy distribution. For example, in the limit $v \to 1$ $(1 - v^2 \ll 1)$, the energy density function for the point impurity becomes almost isotropic except the narrow dip of the width $\sim (1-v^2)^{1/2}$ along the q_x axis. At the same time, the energy density function for the stripe impurity becomes strongly anisotropic in this limit, as has been discussed above.

Even more drastically, the anisotropy of the energy density function influences the total emitted energy

$$E = \int\limits_{-\infty}^{+\infty}\int\limits_{-\infty}^{+\infty} \mathcal{E}(q_x, q_y)\ dq_x dq_y. \tag{12}$$

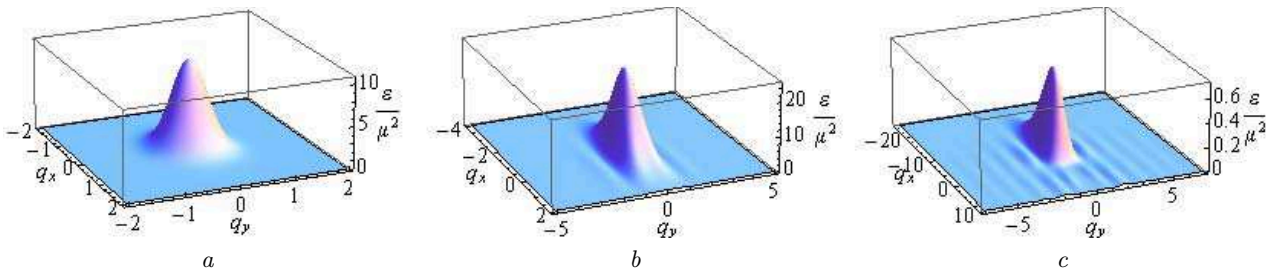

Fig. 1. (Color online) Profile of the energy density $\mathcal{E}(q_x, q_y)$ [see Eq. (11)] for $d = 5$ and $v = 0.3$ (a), $v = 0.7$ (b), $v = 0.99$ (c)

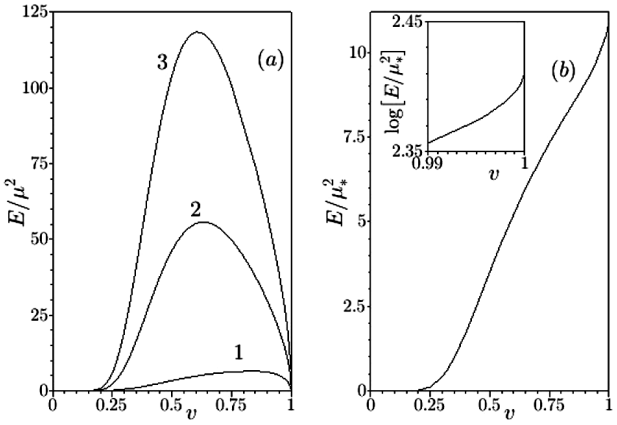

Fig. 2. Dependence of the normalized emitted energy on the fluxon velocity. Panel (a) corresponds to the case of the stripe impurity (2) at $d = 1$ (curve *1*), $d = 5$ (curve *2*) and $d = 10$ (curve *3*). Panel (b) corresponds to the point-impurity case $f(x, y) = \mu_* \delta(x)\delta(y)$ [see the text for details]. The inset shows the details of the $v \to 1$ limit

This integral cannot be computed analytically. Therefore, we have used numerical methods. The energy vs the soliton velocity is shown in Fig. 2. In panel (a), the normalized emitted energy E/μ^2 is shown as a function of the impurity width d. The dependences have a well-defined maximum and tend to zero in the limiting cases $v \to 0$ and $v \to 1$. In the respective 1D problem (e.g., the 1D SG equation) with a δ-like point impurity, the $E(v)$ curve is qualitatively the same [5]. Moreover, the energy density for the 1D case [5] is easily restored, if we formally put $q_y = 0$ in (11). In the zero-velocity limit, the fluxon approaches the impurity with the infinitely small kinetic energy. Therefore, the emitted energy should also be infinitely small. It can be easily shown that, in the $0 < v \ll 1$ limit, the energy grows as $E(v) \sim \exp(-\pi/v)$. In the opposite case as $v \to 1$, the fluxon width tends to zero, so the interaction time will tend to zero as well. As a result, the emitted energy also tends to zero. Thus, there should exist a velocity, for which the energy radiation attains the maximal value. The position of the maximum decreases, as the impurity width increases. This can be explained by the fact that collision with a wider impurity causes the more energy to be emitted. Therefore, a less kinetic energy and, consequently, a smaller velocity are needed in order to reach the maximal radiation. In the limit $d \to 0$, the maximum of the $E(v)$ curve becomes less pronounced and moves toward the value $v = 1$ (and eventually disappears, when $d = 0$), while the total emitted energy tends to zero. This is natural, because the impurity becomes infinitely narrow, while its amplitude remains finite. The soliton energy, however, is proportional to the junction width and is infinitely large for the infinite sample.

In order to restore the point-impurity case, the impurity strength should be redefined as $\mu_* = d\mu$. As a result, in the limit $d \to 0$, the impurity function (2) behaves itself as $f(x, y) \to \mu_* \delta(x)\delta(y)$, and the energy density function (11) turns into Eq. (2.16) of Ref. [19]. The total emitted energy in the point-impurity case as a function of the fluxon velocity is shown in Fig. 2, *b*. The $E(v)$ dependence is a monotonically increasing function that tends to a finite value, as $v \to 1$ (see the inset). Thus, we have obtained the limiting case where the stripe impurity becomes the point impurity, and the maximum of the energy dependence shifts toward $v = 1$ and eventually disappears for $d = 0$.

4. Fluxon Transmission through an Impurity

Now, we consider a more specific situation of a large but finite junction with length $L \gg 1$ and width $w < L$ in the presence of the dissipation and a dc bias [$\alpha > 0$, $\gamma \neq 0$ in Eq. (1)]. The boundary conditions along the y direction are chosen in the von Neumann

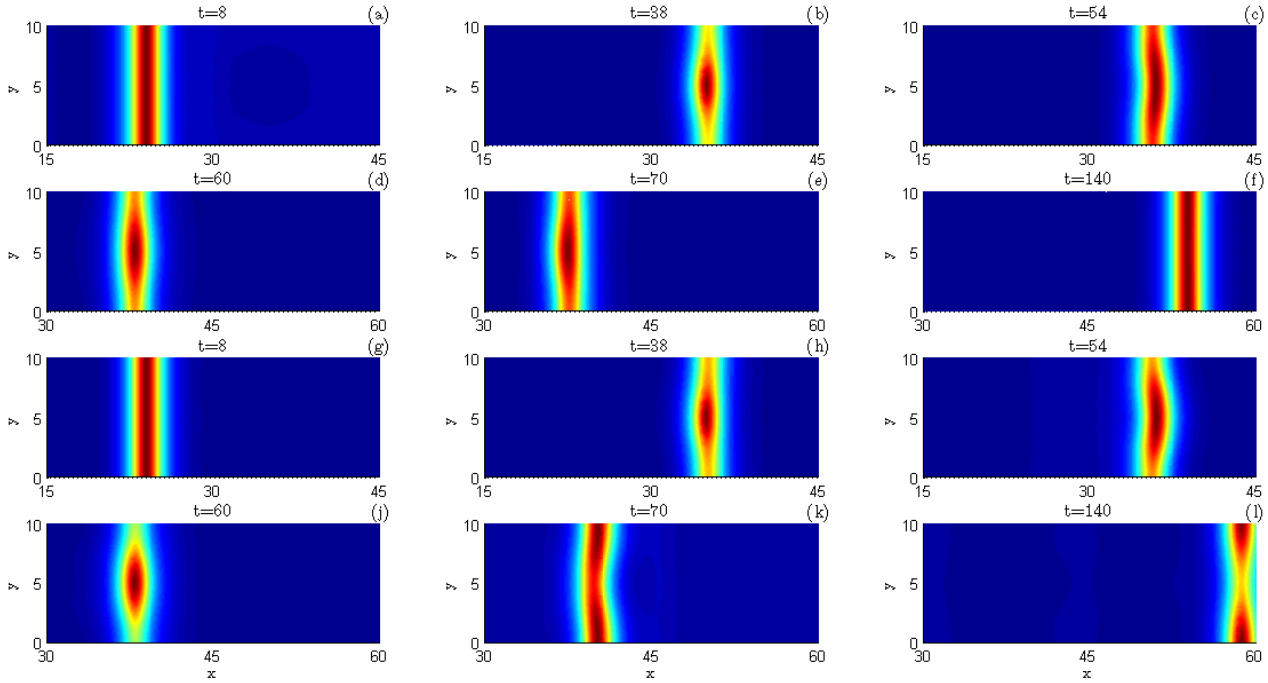

Fig. 3. (Colour online) Contour plot of the time evolution of the Josephson phase derivative $-\partial_t\phi$ in the junction with $L = 70, w = 10$, $\mu = 0.5$, $d = 3$, $\alpha = 0.1$, $\gamma = 0.03$ [(*a*)–(*f*)] and $\alpha = 0.01$, $\gamma = 0.0035$ [(*g*)–(*l*)]. The impurity is placed in the middle of the junction at $x = L/2 = 35$

form: $\partial_y\phi\,(x, -w/2, t) = \partial_y\phi\,(x, w/2, t) = 0$. These boundary conditions are based on the well-known relation $\partial_y\phi \propto -H_x$ [1] and mean the absence of the x-component (H_x) of the external magnetic field. The boundary conditions along the x axis are periodic: $\phi(x + L, y; t) = \phi(x, y; t) + 2\pi$.

First of all, in order to get an idea of the character of the fluxon dynamics, the numerical integration of the 2D SG equation (1) has been carried out. The Josephson phase and its space derivatives are discretized in the following way: $\phi(x, y; t) \to \phi(mh, nh; t) \equiv \phi_{mn}(t)$, $\Delta\phi \simeq h^{-2}\times$ $\times\,(\phi_{m+1,n} + \phi_{m,n+1} + \phi_{m-1,n} + \phi_{m,n-1} - 4\phi_{mn}) +$ $+\mathcal{O}(h^{-4})$, while the δ-function is approximated by the Kronecker δ-symbol. The resulting system of ODEs with boundary conditions was integrated with the use of the 4th order Runge—Kutta scheme. Details of the fluxon interaction with the stripe impurity are given in Fig. 3. It is important to mention that the dissipation in Eq. (1) is crucial, and the soliton interaction with impurities differs from the dissipationless case where the complex resonant behavior occurs [10]. Far away from the impurity, the fluxon exists as only one attractor of the system with the equilibrium velocity (see Ref. [4])

$$v_\infty = \left[1 + \left(\frac{4\alpha}{\pi\gamma}\right)^2\right]^{-1/2}, \tag{13}$$

which is predefined by the damping parameter and the external bias. Therefore, contrary to the non-dissipative case, the transmission consists of only two possible scenarios: passage and trapping.

For the sake of better visualization, the derivative $-\partial_t\phi$ is plotted on the xy plane at the different time moments and for two different dissipation values: $\alpha =$ $= 0.1$ and $\alpha = 0.01$. The fluxon shape experiences certain changes, while it interacts with the obstacle, namely the redistribution of the Josephson phase along the fluxon line in the y direction. A certain bending of the fluxon shape in the same direction can be observed as well. These distortions eventually die out after some time. For $\alpha = 0.1$, this happens quite soon after the passage through the impurity. For a smaller dissipation ($\alpha = 0.01$, as shown in Figs. 3, *g*–*l*), the oscillations of the Josephson phase along the y

direction seem to survive for a much longer time, comparable with the fluxon propagation time along the junction. The numerical simulations for thinner junctions, $w < 10$ (not shown in the paper), demonstrate that these shape distortions are considerably weaker. Moreover, no significant radiation was observed as a result of the fluxon-impurity interaction, because the fluxon velocity in this case is around $v_\infty \sim 0.2$. As Fig. 2 suggests, the emitted radiation in this velocity range is negligibly small. Thus, when studying the 2D fluxon interaction with impurities, one can assume with a high degree of certainty that the fluxon is an almost hard rod at least if $w \sim \mathcal{O}(1)$ and $\alpha \gtrsim 0.1$. Due to the finiteness of the junction in the y direction and the von Neumann boundary conditions, the straight soliton front is the energetically most favourable solution, and, thus, it is not possible to observe the arc-like solitons reported in [19].

Similarly to the fluxon propagation in the 1D LJJ [4, 5, 7], there must exist two characteristic values of the bias current, the critical current $\gamma_{\rm c}$, and the *retrapping* current $\gamma_{\rm thr}$, $\gamma_{\rm c} > \gamma_{\rm thr}$. If $\gamma > \gamma_{\rm c}$, the pinning on the impurity is not possible, and there exists only one attractor that corresponds to the fluxon propagation. This happens because the bias current is too strong for the fluxon to get trapped on the impurity. In the interval $\gamma_{\rm thr} < \gamma < \gamma_{\rm c}$, two attractors coexist: one corresponds to the fluxon being pinned on the impurity and another one to the fluxon propagation. If $\gamma < \gamma_{\rm thr}$, the only possible regime is the fluxon pinning on the impurity. Thus, the retrapping current is the minimal bias current, for which the fluxon propagation is still possible. By varying γ, one observes the hysteresis: when the bias is increased from $\gamma = 0$ to $\gamma = \gamma_{\rm c}$, the fluxon stays pinned and begins to move if $\gamma > \gamma_{\rm c}$; it continues to move, when the bias is now slowly decreased, and gets trapped back on the impurity at $\gamma = \gamma_{\rm thr}$. The value of $\gamma_{\rm c} = 4\mu/(3\sqrt{3}\pi)$ is defined only by the properties of the impurity, does not depend on α (because the fixed point that corresponds to the trapped fluxon ceases to exist if $\gamma > \gamma_{\rm c}$), and can be obtained directly from the 1D analog. Contrary, for the retrapping current, the dimensionality of the junction and its width are crucial.

Far from the impurity, the fluxon kinetic energy is proportional to the junction width and equals $E_k = 8w[(1-v_\infty^2)^{-1/2} - 1]$. In the non-relativistic fluxon case ($|v_\infty| \ll 1$), one gets $v_\infty \simeq \pi\gamma/(4\alpha)$. We can use the point-particle ansatz, where the fluxon center-of-mass coordinate $X(y,t)$ is substituted instead of the vt term in the exact solution (3) of the unperturbed SG equation. The substitution of this ansatz in Eq. (1) yields the Newtonian equation of motion for the fluxon center of mass. Our aim here is to determine the retrapping current. Thus, the non-relativistic limit, where no significant radiation is expected, can be used. Therefore, there is no radiation term in the above ansatz.

Since the fluxons under consideration are extended objects in the y direction, the equation for the center-of-mass dynamics, as well as the impurity potential, should depend on y. With regard for the numerical simulations, we consider the fluxon as an absolutely rigid rod. Therefore, the fluxon center-of-mass dynamics can be effectively projected on the x axis, and the respective equation of motion can be written as

$$m\ddot{X} + m\alpha\dot{X} + \partial_X U(X) = 0,$$

$$U(X) = -2\pi\gamma X + U_0(X) = -2\pi\gamma X + \frac{2\mu}{\cosh^2 X}, \quad (14)$$

where m is the fluxon mass, and the center-of-mass coordinate X depends only on the time. The potential $U(X)$ has a minimum at $X_{\rm min} \simeq -\ln(\mu/\gamma)/2$ and a maximum $X_{\rm max} > X_{\rm min}$, $X_{\rm max} \simeq -\pi\gamma/(2\mu)$. Because of the bias γ, the potential is asymmetric with respect to the minimum, and the fluxon slows down, when approaching the impurity (see Figs. 3, *b*–*e*, where the fluxon spends a lot of time in a neighborhood of the impurity at $x = L/2$) but quickly accelerates back to the equilibrium velocity after passing it.

In the pure 1D case, the fluxon mass $m = 8$. In order to project the problem on the 1D picture, it is necessary to rescale the mass. Indeed, within the collective-coordinate approach, the fluxon is considered to be a rigid rod sliding down in the potential $U(X)$ that does not depend on the impurity width d. However, only the central part of this rod with $-d/2 < y < d/2$ interacts with the impurity, while the "tails" of the rod at $d/2 < |y| < w/2$ do not. This is taken into account if the fluxon mass is defined as $m = 8w/d$. When the impurity length stretches across the whole junction, i.e. $d = w$, the problem becomes completely independent of the y direction, and, consequently, the mass equals $m = 8$. These considerations are approximate, because the fluxon bending on the boundaries of the impurity

has been neglected. Thus, within the kinematic approach, the retrapping current can be found as a root of the energy balance equation $E_k = 2\mu$, where $E_k = m[(1-v_\infty^2)^{-1/2} - 1] \simeq 4wv_\infty^2/d + \mathcal{O}(v_\infty^4)$ is the fluxon kinetic energy. In the non-relativistic case, one gets $\gamma_{thr} \simeq (\alpha/\pi)\sqrt{8\mu d/w}$. The correction of the order $\mathcal{O}(\alpha^2)$ can be taken into account with the help of the method developed in [5]. Its modification for the 2D case is straightforward, so only the principal points are mentioned here. The corrected energy balance relation equates the fluxon energy at $X = -\infty$ and its losses due to the dissipation, ΔE, with the maximal height of the potential barrier $U(X)$:

$$m\left(\frac{\pi\gamma}{2\alpha}\right)^2 + \Delta E = U(X_{\max}). \tag{15}$$

As a result of the dissipation, the fluxon loses the energy:

$$\Delta E = \frac{8\alpha w}{d}\int\limits_{-\infty}^{X_{\max}} (v_\infty - \dot{X})dX \simeq 4\alpha\ln 2\ (2\mu w/d)^{1/2}. \tag{16}$$

Here, $\dot{X}(t) \simeq -(\mu d/2w)^{1/2}(1+\tanh X)$ is an approximate solution of Eqs. (14). Inserting this correction term ΔE into the improved energy balance equation (15) and keeping the terms up to the order $\mathcal{O}(\alpha^2)$, one gets the final formula for the retrapping current:

$$\gamma_{\rm thr} \simeq \frac{\alpha}{\pi}\left[\left(\frac{8\mu d}{w}\right)^{1/2} - 4\alpha\ln 2\right]. \tag{17}$$

From this expression, one can clearly see that if only the $\mathcal{O}(\alpha)$ term is taken into account, the retrapping current disappears as $w \to \infty$. Thus, in the infinitely wide junction, a fluxon always passes the impurity. The second term in Eq. (17) does not depend on w, and, therefore, it may lead to the erroneous conclusion that γ_{thr} does not tend to zero, as $w \to \infty$. However, it should be noted that this term has been derived under the assumption of w being finite.

The numerical simulations confirm that the retrapping current decays with the growth of the junction width (as shown in Fig. 4). Expression (17) appears to be in good agreement with the numerical data. Similarly to the point impurity case, the discrepancy between the analytical and numerical results increases at larger w. In the limit $d/w \to 1$, the effective 1D picture is restored because the impurity stripe crosses the whole junction in the y direction. Thus, the retrapping current attains the value

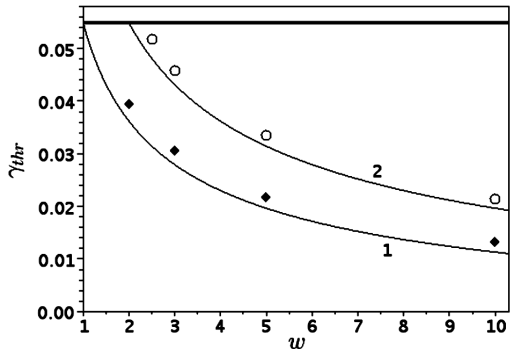

Fig. 4. Retrapping current as a function of the junction width w for $\alpha = 0.1$, $\mu = 0.5$, $d = 1$ (1 and ♦) and $d = 2$ (2 and ∘). Markers correspond to the numerical results and solid lines correspond to the approximation (17). Thick horizontal line corresponds to the retrapping current on the point microshort in the pure 1D case

$\gamma_{\rm thr} = \alpha(\sqrt{8\mu} - 4\alpha\ln 2)/\pi$ for the 1D soliton case (shown by the thick horizontal line in Fig. 4, *b*). Thus, we observe that if the stripe impurity constitutes, for example, about 1/3 of the junction width, the retrapping current is about 40% less than the respective 1D value. In the case of the 2D point impurity problem, the strength μ should be redefined as $\mu_* = \mu d$, and the retrapping current will be still defined as that in Eq. (17).

The following simple argument that explains the enhanced fluxon transmission across the obstacle of width d in a 2D LJJ can be formulated. The impurity can be described as a localized potential barrier. Only the central part ($|y| \gtrsim d/2$) of the fluxon initially homogeneous in the y direction takes part in the interaction process, while the marginal areas $d/2 \lesssim |y| \le w/2$ do not. Thus, if the energy in the tails is sufficient enough to overcome the barrier, the fluxon will pass. If $w \to \infty$, the energy in the non-interacting part of the fluxon tends to infinity, and, consequently, it will overcome any localized obstacle.

5. The Current-Voltage Characteristics

With the help of the results obtained in the previous sections, we can now proceed with the construction of the current-voltage characteristics (CVCs) of a finite-size LJJ ($L, w \gg 1$) with one fluxon trapped in it. The considerations below apply both to an annular junction [22] (an additional constraint $L \gg w$ should be applied in order to justify the neglecting of the curvature effects) or to a linear one [23]. For the

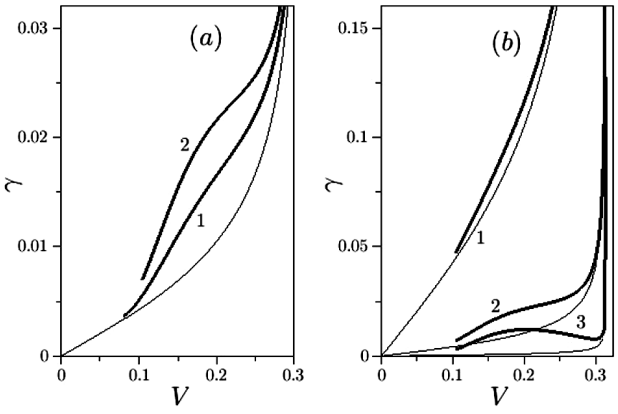

Fig. 5. Current-voltage characteristics for the LJJ with $L = 20$, $w = 10$, $\mu = 0.5$. Panel (a) corresponds to the parameter values $\alpha = 0.01$, $d = 3$ (curve *1*), and $d = 5$ (curve *2*) while panel (b) corresponds to the values $d = 5$, $\alpha = 0.1$ (curve *1*), $\alpha = 0.01$ (curve *2*) and $\alpha = 0.001$ (curve *3*). The thin unmarked curves correspond to the homogeneous case $\mu = 0$ for the respective values of α

annular junction, the boundary conditions (b.c.) are given in the previous section, while, for the linear junction, the periodic b.c. should be replaced by the von Neumann conditions $\partial_x\phi(\pm L/2, y, t) = 0$.

If the fluxon is moving in the LJJ, it generates the voltage drop, which equals $V = 2\pi v/L$ after the averaging over large times, where v is its average velocity. The total power (energy per time unit) produced by the dc bias $P_{\rm tot} = V\gamma Lw$ should balance the dissipative loss $P_{\rm diss}$ and the radiative loss $P_{\rm rad}$: $P_{\rm tot} = P_{\rm diss} + P_{\rm rad}$. The radiative loss power has been computed in Ref. [4] for a 1D junction. In the 2D case, it equals $P_{\rm diss} = 8\alpha w v^2/\sqrt{1-v^2}$. The radiative power loss on large times equals $P_{\rm rad} = E(v)/T = E(v)v/L$, where $T = L/v$ is the time interval between two consecutive fluxon-impurity scattering events, and $E(v)$ is the radiation energy emitted during such an event. This energy is given by Eqs. (11)–(12) [1]. As a result, the power balance equation yields the CVC

$$\gamma = \frac{1}{2\pi}\left\{\frac{4\alpha LV}{\pi}\left[1-\left(\frac{LV}{2\pi}\right)^2\right]^{-1/2} + \frac{E(LV/2\pi)}{Lw}\right\}, \quad (18)$$

where $V = 2\pi v/L$ is the average voltage drop across the junction. This expression is defined in the interval $\gamma_{\rm thr} < \gamma < \infty$, where $\gamma_{\rm thr}$ is given by Eq. (17). We note that, in experiments, one of the quantities (γ or V) is controlled, and another one is measured.

In Fig. 5, CVCs (18) are plotted. It appears that these curves depend strongly on the junction parameters. The thin unmarked lines are the CVCs for a spatially homogeneous junction ($\mu = 0$), which have been obtained from Eq. (18), when the second term is absent. In such a case, the equilibrium fluxon velocity v_∞ is recovered easily. The emitted radiation results in a deviation of the CVC from the homogeneous limit. This deviation is noticeable for the intermediate values of the voltage (fluxon velocity) but decreases in the limits $V \to 0$ and $V \to 2\pi/L$ ($v \to 1$). The deviation from the homogeneous limit increases if the impurity width d is increased or when the junction area Lw is decreased. It also can be increased if the dissipation is decreased (see Fig. 5, b). For very small values of α, the CVC can even have a local maximum. This behavior of CVCs occurs, because while the first term in (18) is a monotonically increasing function of V, the second ("radiative") term has a clear maximum as shown in Fig. 2. The proper parameter choice can result in the domination of the second term and the appearance of a local maximum. It should be noted, however, that the realistic dissipation values lie in the interval $\alpha \sim 0.01 - 0.1$; thus, observation of this maxima is rather unlikely. The abrupt ending of the CVCs is due to the fact that, for the bias $\gamma < \gamma_{\rm thr}$, the fluxon is always trapped by the impurity and, consequently, it produces the zero voltage drop. Finally, the critical current $\gamma_{\rm c} = 4\mu/(\pi 3\sqrt{3}) \simeq 0.1225$ for $\mu = 0.5$ corresponds to the rather large fluxon velocities, which are close to the ultrarelativistic limit $v \to 1$.

6. Conclusion

We have shown that the two-dimensional fluxon passage across microshorts is significantly enhanced in comparison with that in the purely one-dimensional case. The retrapping threshold current decays with the junction width approximately as $w^{-1/2}$, according to the kinematic approach. The numerical sim-

[1] We make two assumptions. First of all, the radiated energy has been defined for the infinite junction. For a finite junction, the continuous spectrum (11) should be replaced by a discrete one. However, if the junction is large enough, this difference is negligible. Secondly, this energy has been calculated in the dissipationless case ($\alpha = 0$). Nevertheless, most of the energy is emitted during the finite time of the fluxon-impurity interaction, and if $\alpha \ll 1$, the dissipation of the emitted waves is very small. Especially, this is true, when v is not small, and the interaction time is $\mathcal{O}(v^{-1})$.

ulations support this dependence, while the discrepancy between the numerical simulations and the analytical calculations is explained by the fact that, for $w \gg 1$, the fluxon cannot be longer considered as a completely rigid object, and its deformation in the y direction should be taken into account.

The energy of the radiation emitted during the fluxon-impurity scattering process shows a clear resonant behavior as a function of the fluxon velocity v. There exists an optimal velocity, for which the radiated energy is maximal, and, at the same time, this energy decreases to zero in the limits $v \to 0$ and $v \to 1$. Such a dependence was observed for the purely 1D fluxon scattering problem on the δ-like point impurity [5, 6]. On the other hand, our result is in the sharp contrast with the 2D fluxon scattering on the δ-like point impurity [19] (described as $f(x,y) = \mu_* \delta(x)\delta(y)$ in the SG equation), where the emitted energy grows in the monotonic way from the zero value at $v = 0$ to some constant at $v = 1$. Thus, in our opinion, the stripe-like approximation of the impurity appears to be more realistic.

We have constructed the current-voltage characteristics (CVCs) of the large but finite junctions with the stripe impurity. The role of the emitted radiation can be easily spotted on such a CVC as a deviation from the CVC of a homogeneous junction. These characteristics can be measured experimentally.

One of the authors (Y.Z.) acknowledges the financial support from the Ukrainian State Grant for Fundamental Research No. 0112U000056.

APPENDIX

In this appendix, we present the details of the calculation of the emitted radiation.

Representation (8) is substituted into the linearized equation of motion (4). As a result, we obtain

$$\int\limits_{-\infty}^{+\infty}\int\limits_{-\infty}^{+\infty} \left[\partial_\tau^2 a + \bar{\omega}^2 a\right] \varphi(\xi, y; q_\xi, q_y) dq_\xi dq_y =$$

$$= 2F(\xi, y, \tau) \tanh\xi \ \cosh^{-1}\xi, \tag{19}$$

$$\bar{\omega} = (1 + q_\xi^2 + q_y^2)^{1/2}. \tag{20}$$

The function $F(\xi, y, \tau)$ is given by Eq. (6). It is more convenient to work with another radiation amplitude,

$$b(q_\xi, q_y; \tau) \doteq (\partial_\tau a - i\bar{\omega} a) e^{i\bar{\omega}\tau}, \tag{21}$$

that satisfies $\partial_\tau b = e^{i\bar{\omega}\tau}\left(\partial_\tau^2 + \bar{\omega}^2\right) a$. We multiply both the sides of Eq. (19) by $\varphi^*(\xi, y; q'_\xi, q'_y)$ and integrate them as $\int_{-\infty}^{+\infty}\int_{-\infty}^{+\infty} d\xi dy$. Using the orthogonality condition

$$\int\limits_{-\infty}^{+\infty}\int\limits_{-\infty}^{+\infty} \varphi^*(\xi, y; q_\xi, q_y)\varphi(\xi, y; q'_\xi, q'_y)\ d\xi dy =$$

$$= \delta(q_\xi - q'_\xi)\ \delta(q_y - q'_y) \tag{22}$$

and making some calculations, we obtain

$$\partial_\tau b = \frac{e^{i\bar{\omega}\tau}}{\sqrt{2\pi}} \int\limits_{-\infty}^{+\infty}\int\limits_{-\infty}^{+\infty} F(\xi, \tau, y) e^{-i(q_\xi \xi + q_y y)} \times$$

$$\times \frac{\tanh\xi}{\cosh\xi} \frac{q_\xi - i\tanh\xi}{(1+q_\xi^2)^{1/2}}\ d\xi\ dy =$$

$$= -\frac{4\mu}{(2\pi)^{1/2}} \left(\frac{1-v^2}{1+q_\xi^2}\right)^{1/2} \frac{\sin(q_y d/2)}{q_y} e^{i(\bar{\omega} + q_\xi v)\tau} \times$$

$$\times \frac{\tanh v\tau}{\cosh v\tau} (q_\xi + i\tanh v\tau). \tag{23}$$

1. A. Barone and G. Paterno, *Physics and Applications of the Josephson Effect* (Wiley, New York, 1982).
2. K.K. Likharev, *Dynamics of Josephson Junctions and Circuits* (Gordon and Breach, New York, 1986).
3. A.V. Ustinov, Physica D **123**, 315 (1998).
4. D.W. McLaughlin and A.C. Scott, Phys. Rev. A **18**, 1652 (1978).
5. Yu.S. Kivshar, B.A. Malomed, and A.A Nepomnyashchy, Sov. Phys. JETP **67**, 850 (1988); Yu.S. Kivshar and B.A. Malomed, Phys. Lett. A **129**, 443 (1988).
6. M.B. Mineev, M.V. Feigel'man, and V.V. Shmidt, Sov. Phys. JETP **54**, 155 (1981).
7. B.A. Malomed and A.V. Ustinov, J. Appl. Phys. **67**, 3791 (1990).
8. S. Sakai, H. Akoh, and H. Hayakawa, Japan. J. Appl. Phys. **24**, L771 (1985); H. Akoh, S. Sakai, A. Yagi, and H. Hayakawa, IEEE Trans. Magn. **21**, 737 (1985); I.L. Serpuchenko and A.V. Ustinov, Sov. Phys. JETP Lett. **46**, 549 (1987).
9. M.B. Fogel, S.E. Trullinger, A.R. Bishop, and I.A. Krumhansl, Phys. Rev. Lett. **36**, 1411 (1976).
10. Y.S. Kivshar, Z. Fei, and L. Vazquez, Phys. Rev. Lett. **67**, 1177 (1991); Y.S. Kivshar *et al.*, J. Phys. A: Math. Gen. **25**, 5711 (1992).
11. E. Goldobin *et al.*, Phys. Rev. B **72**, 054527 (2005); A. Fedorov, A. Shnirman, G. Schön, and G.S.A. Kidiyarova-Shevchenko, Phys. Rev. B **75**, 224504 (2007).
12. P.L. Christiansen and O.H. Olsen, Phys. Lett. A **68**, 185 (1978); P.L. Christiansen and P.S. Lomdahl, Physica D **2**, 482 (1981).
13. J. Geicke, Physica Scripta **29**, 431 (1984).
14. B.A. Malomed, Physica D **24**, 155 (1987).
15. B. Piette and W.J. Zakrzewski, and J. Brand, J. Phys. A: Math. Gen. **38**, 10403 (2005).
16. A. Benabdallah, J.G. Caputo, and N. Flytzanis, Physica D **161**, 79 (2002).

17. J.G. Caputo and Y. Gaididei, Physica C **402**, 160 (2004).
18. Y. Zolotaryuk, A.V. Savin, and P.L. Christiansen, Phys. Rev. B **57**, 14213 (1998).
19. B.A. Malomed, Physica D **52**, 157 (1991).
20. D.R. Gulevich *et al.*, Phys. Rev. Lett. **101**, 127002 (2008); Phys. Rev. B **80**, 094509 (2008).
21. J. Rubinstein, J. Math. Phys. **11**, 258 (1970); M. Salerno, E. Joergensen, and M.R. Samuelsen, Phys. Rev. B **30**, 2635 (1984).
22. A. Davidson, B. Dueholm, B. Krygger, and N.F. Pedersen, Phys. Rev. Lett. **55**, 2059 (1985).
23. A. Fulton and R.C. Dynes, Solid State Commun. **12**, 57 (1973).

Received 18.04.13

І.О. Стародуб, Я. Золотарюк

РОЗСІЯННЯ ФЛЮКСОНА
НА ПОЛОСОПОДІБНІЙ ДОМІШЦІ У ДВОВИМІРНОМУ ДЖОЗЕФСОНІВСЬКОМУ ПЕРЕХОДІ

Р е з ю м е

Досліджено взаємодію солітона (флюксона) з полосоподібною неоднорідністю у двовимірному джозефсонівському переході. Розраховано випромінення, викликане розсіюванням флюксона на домішці. Повна випромінена енергія має чітко виражену резонансну залежність від швидкості флюксона. Знайдено чисельно та аналітично струм закріплення на домішці як функцію ширини переходу. Обчислювальні дані добре узгоджуються з аналітичними передбаченнями.